

---

# GRAPH LEARNING IN 4D: A QUATERNION-VALUED LAPLACIAN TO ENHANCE SPECTRAL GCNs

---

A PREPRINT

**Stefano Fiorini**  
Italian Institute of Technology  
Genoa, Italy  
stefano.fiorini@iit.it

**Stefano Coniglio**  
University of Bergamo  
Bergamo, Italy  
stefano.coniglio@unibg.it

**Michele Ciavotta**  
University of Milano-Bicocca  
Milan, Italy  
michele.ciavotta@unimib.it

**Enza Messina**  
University of Milano-Bicocca  
Milan, Italy  
enza.messina@unimib.it

1st January 2024

## ABSTRACT

We introduce *QuaterGCN*, a spectral Graph Convolutional Network (GCN) with quaternion-valued weights at whose core lies the *Quaternionic Laplacian*, a quaternion-valued Laplacian matrix by whose proposal we generalize two widely-used Laplacian matrices: the *classical Laplacian* (defined for undirected graphs) and the complex-valued *Sign-Magnetic Laplacian* (proposed to handle digraphs with weights of arbitrary sign). In addition to its generality, our Quaternionic Laplacian is the only Laplacian to completely preserve the topology of a digraph, as it can handle graphs and digraphs containing antiparallel pairs of edges (digons) of different weights without reducing them to a single (directed or undirected) edge as done with other Laplacians. Experimental results show the superior performance of QuaterGCN compared to other state-of-the-art GCNs, particularly in scenarios where the information the digons carry is crucial to successfully address the task at hand.

## 1 Introduction

Deep Learning (DL) has recently achieved a striking success, contributing to the advancement of several research areas such as natural language processing [Vaswani et al., 2017], business intelligence [Khan et al., 2020], and cybersecurity [Dixit and Silakari, 2021], only to name a few. While many of the most popular DL architectures are designed to process data arranged in grid-like structures (such as RGB pixels in 2D images and video streams), many real-world phenomena are ruled by more general relationships that are better represented by a graph [Bronstein et al., 2017]. For example, e-commerce relies on graphs to model the user-product interaction to make recommendations, drug discovery models molecule bioactivity via interaction graphs, and information discovery uses multi-relational knowledge graphs to extract information between the entities [Ye et al., 2022].

Graph Convolutional Networks (GCNs) model the interaction between the entities of a complex system via a graph-based *convolution operator*. They are the primary tool for machine learning tasks on data that enjoy a graph-like structure. In spatial GCNs, the convolution operator is defined as a localized aggregation operator [Xu et al., 2018]. There are various implementations and extensions of this operator. E.g., in attention-based GCNs the convolutional operator is used to dynamically learn attention scores on the graph edges [Veličković et al., 2018], while, in recurrence-based GCNs, the operator leverages gated recurrent units to capture edge-specific information and temporal dependencies during message passing [Li et al., 2016].

While spatial GCNs rely on different heuristics for the definition of their convolution operator, *spectral* GCNs are solidly grounded in signal and algebraic graph theory. They rely on a convolution operator based on a Fourier transform

Table 1: Main differences between Laplacian matrices used in spectral GCN literature. For a graph with edge set  $E$ ,  $w_1$  and  $w_2$  denote the weights of the digons  $(u, v), (v, u) \in E$ .

Laplacian Symbol	Proposed in	Number System	Allows Negative Edge Weights?	Allows Digons?			
				if $w_1 = w_2$	if $w_1 = -w_2$	if $w_1 \neq w_2$	if $w_1 \neq -w_2$
$L$	Kipf and Welling [2017]	$\mathbb{R}$	✗	✓	✗	✗	✗
$L^{(q)}$	Zhang et al. [2021a]	$\mathbb{C}$	✗	✓	✗	✗	✗
$L^\sigma$	Fiorini et al. [2022]	$\mathbb{C}$	✓	✓	✗	✗	✗
$L^{(q)}$	He et al. [2022b]	$\mathbb{C}$	✓	✓	✗	✗	✗
$L^{(q)}$	Ko [2022]	$\mathbb{C}$	✓	✓	✓	✗	✗
$L^\vartheta$	<b>This paper</b>	$\mathbb{H}$	✓	✓	✓	✓	✓

applied to the eigenspace of the Laplacian matrix of the graph [Kipf and Welling, 2017, He et al., 2022a, Wu et al., 2022] to capture the global structure of the graph. Spectral GCNs have been shown to achieve superior performance to their spatial-based counterpart in a number of papers, see, e.g., Zhang et al. [2021a], Fiorini et al. [2022]. Our focus in the paper will be on extending the applicability of spectral GCNs. Spatial GCNs will be considered only for comparison purposes within computational experiments.

Despite the growing interest in academia and industry alike for neural-network methods suitable for progressively more general classes of graphs, the literature on spectral GCNs has only recently begun to include extensions beyond the basic case of unweighted, undirected graphs. As a result, the adoption of spectral GCNs in learning tasks involving graphs such as those featuring directed edges, digons, and edges with negative weights [He et al., 2022a, Wu et al., 2022] is still limited. To (partially) address such limitations, alternative notions of the Laplacian matrix have been put forward, among which the *Magnetic Laplacian* [Lieb and Loss, 1993], which was originally proposed in physics and first used within a spectral GCN in [Zhang et al., 2021a], albeit with the limitation of only handling digraphs non-negative edge weights. Spectral-based GCNs suitable for digraphs with weights of unrestricted sign have been proposed only recently. Three such networks are SigMaNet [Fiorini et al., 2022] (based on the therein proposed *Sign-Magnetic Laplacian*), MSG-NN [He et al., 2022b] (based on an extension of the *Magnetic Laplacian*), and the network proposed in [Ko, 2022].

Graphs with *digons* (pairs of antiparallel directed edges) occur in many important applications including, e.g., traffic and networking and, so far, have eluded every spectral-based GCN proposed in the literature. Indeed, to the best of our knowledge none of the known spectral-based GCNs can handle graphs with digons with arbitrary weights and signs without collapsing them to single edges (either directed or undirected), which often results in destroying any topological information such digons may carry.

In this work, we extend the theory of spectral GCNs to digraphs with unrestricted edge weights also including digons. This is achieved by introducing the *Quaternionic Laplacian*  $L^\vartheta$ , the first, to our knowledge, graph Laplacian matrix with quaternion-valued entries.<sup>1</sup> We prove that  $L^\vartheta$  generalizes different previously proposed Laplacians (both real- and complex-valued), that it satisfies all the properties that are needed to build a convolutional operator around it, and that it can naturally represent digons in such a way that the graph can be fully reconstructed from it without any loss of topological information. Around the Quaternionic Laplacian, we design QuaterGCN, a spectral GCN which relies on both  $L^\vartheta$  and quaternion-valued network weights.

While some GCNs employing quaternion weights have been recently proposed [Nguyen et al., 2021, Wang et al., 2022, Le et al., 2023], only QGNN, proposed by Nguyen et al. [2021], is spectral based. As QGNN relies on the classical convolution operator of Kipf and Welling [2017] bases on the classical (real-valued) graph Laplacian, it fails to fully capture the whole graph topology unless the graph has non-negative edge weights and is undirected (which implies that it contains no digons).

We summarize the differences between the Quaternionic Laplacian  $L^\vartheta$  we introduce in this work and previous proposals in Table 1. For each Laplacian, the table reports the paper in which it was proposed or used within a spectral GCN and the corresponding symbol (which is often reused with some overload). It also indicates the type of number system associated with each Laplacian and its capability to handle edges with negative weights and digons.

## Main Contributions of The Work

<sup>1</sup>The letter  $\vartheta$  in  $L^\vartheta$  is an archaic Greek letter often replaced in modern text by the Latin letter "q" as in "quaternion".

- We propose the quaternion-valued Quaternionic Laplacian matrix  $L^q$ , which naturally captures the presence of digons of different weight (*asymmetric*) without reducing them to a single edge as done in many previously-proposed Laplacians.
- We prove that  $L^q$  generalizes both the standard Laplacian and the Sign-Magnetic Laplacian, as it coincides with the former when  $G$  is undirected and with the latter when  $G$  features directed edges with weights of arbitrary sign and all its digons have the same weight (*symmetric*).
- We incorporate  $L^q$  into QuaterGCN, a spectral-based GCN that includes quaternion-valued convolutional layers and quaternion-valued network weights.
- Our experiments demonstrate that QuaterGCN consistently outperforms state-of-the-art spatial and spectral GCNs, particularly on tasks and datasets where the information carried by the digons is critical.

## 2 Preliminaries and Previous Works

Let  $G = (V, E)$  be an undirected graph with  $n = |V|$  vertices without weights nor signs associated with its edges and let  $A \in \{0, 1\}^{n \times n}$  be its adjacency matrix. The *classical Laplacian matrix*  $L \in \mathbb{Z}_+^{n \times n}$  of  $G$  is defined as  $L := D - A$ , where  $D := \text{diag}(Ae)$  is the degree matrix of  $G$ ,  $e$  is the all-one vector of appropriate size, and the operator  $\text{diag}$  builds a diagonal matrix with the argument on the main diagonal. The normalized version of  $L$  is defined as  $L_{\text{norm}} := D^{-\frac{1}{2}}(D - A)D^{-\frac{1}{2}} = I - D^{-\frac{1}{2}}AD^{-\frac{1}{2}}$ .

For a spectral convolution operator to be well-defined, the graph Laplacian must fulfill three properties: **P.1**) it must be diagonalizable, i.e., it must admit an eigenvalue decomposition; **P.2**) it must be positive semidefinite; **P.3**) its spectrum must be upper-bounded by 2 [Kipf and Welling, 2017].

While  $L$  and  $L_{\text{norm}}$  always satisfy such properties if  $G$  is undirected (i.e.,  $A$  is symmetric) and has nonnegative edge weights (i.e.,  $A$  is component-wise nonnegative), this is not always the case for more general graphs. When  $G$  is a digraph,  $L$  is sometimes defined as a function of  $A_s := \frac{1}{2}(A^\top + A)$  and  $D_s := \text{Diag}(A_s e)$ , rather than of  $A$  and  $D$ . This is, e.g., the case of QGNN [Nguyen et al., 2021]. While such a choice preserves the mathematical properties of  $L$ , it significantly alters the topology of the graph. Indeed, when general graphs are considered, the following issues may arise:

- **Issue 1.** If  $G$  is a digraph, defining  $L$  as a function of  $A_s$  is equivalent to transforming the original graph into an undirected version of it, losing any directional information the original graph contained.
- **Issue 2.** If  $G$  features negative-weighted edges, neither  $A$  nor  $A_s$  belong, in general, to  $\mathbb{Z}_+^{n \times n}$ . This can lead to  $D_{uu} < 0$  for some  $u \in V$ , in which case  $L$  is not well defined in  $\mathbb{Z}_+^{n \times n}$  due to  $D^{-\frac{1}{2}}$  being irrational.
- **Issue 3.** If  $G$  contains asymmetric digons, the weight asymmetry is completely lost in  $A_s$ , since the latter only features the average of the two weights. For example, in an author-citation graph, a digon representing two authors, the first one citing the second one 50 times while being cited by them only 2 times, would be identical to the two authors symmetrically citing each other precisely 26 times.

**Issue 1** was first addressed by Zhang et al. [2021a,b] by introducing Magnet, a spectral GCN relying on the *Magnetic Laplacian*  $L^{(q)}$ . Such a Laplacian is a complex-valued extension of  $L$  to unweighted directed graphs, and was originally proposed within an electro-magnetic charge model by Lieb and Loss [1993]. It is defined as follows:

$$\begin{aligned} L^{(q)} &:= D_s - H^{(q)}, \quad \text{with} \\ H^{(q)} &:= A_s \odot \exp(\mathbf{i} \Theta^{(q)}), \quad \Theta^{(q)} := 2\pi q (A - A^\top), \end{aligned}$$

where  $\odot$  denotes the Hadamard product,  $\mathbf{i} = \sqrt{-1}$ ,  $\Theta$  is a phase matrix that encodes the edge directions, and  $\exp(\mathbf{i} \Theta^{(q)}) := \cos(\Theta^{(q)}) + \mathbf{i} \sin(\Theta^{(q)})$ , where  $\cos$  and  $\sin$  are applied component-wise. The parameter  $q \in \mathbb{R}_0^+$  is usually chosen in  $[0, \frac{1}{4}]$  or  $[0, \frac{1}{2}]$  [Zhang et al. [2021a], Fanuel et al. [2017]]. Choosing  $q = 0$  implies  $\Theta^{(q)} = 0$  and thus  $L^{(q)}$  boils down to the Laplacian matrix  $L$  defined on  $A_s$  (in which case the directionality of  $G$  is lost).

**Issue 2** was first addressed by Fiorini et al. [2022] via the introduction of the spectral GCN SigMaNet and the *Sign-Magnetic Laplacian*  $L^\sigma$ . Unlike  $L^{(q)}$ ,  $L^\sigma$  is well defined for graphs with negative edge weights and enjoys some robustness properties to weight scaling (which in  $L^{(q)}$  could artificially alter the sign pattern of  $\Theta$  and thus the directionality of the edges).  $L^\sigma$  is defined as follows:

$$\begin{aligned} L^\sigma &:= \bar{D}_s - H^\sigma, \quad \text{with} \\ H^\sigma &:= A_s \odot \left( ee^\top - \text{sgn}(|A - A^\top|) + \mathbf{i} \text{sgn}(|A| - |A^\top|) \right), \end{aligned}$$

where  $\bar{D}_s := \text{Diag}(|A_s| e)$  and  $\text{sgn} : \mathbb{R} \rightarrow \{-1, 0, 1\}$  is the *signum* function applied component-wise. After Fiorini et al. [2022], He et al. [2022b] extended the Magnetic Laplacian as a function of  $\bar{D}_s := \text{Diag}(\frac{|A|+|A|^\top}{2} e)$  rather than  $D_s$ . This Laplacian is well-defined for graphs with negative edge weights, but it still suffers from the scaling issue pointed out by Fiorini et al. [2022] which  $L^\sigma$  avoids.

**Issue 3**, to the best of our knowledge, has not yet been addressed. We set ourselves out to do so in this paper.

### 3 A Quaternion-Valued Laplacian

In this section, we introduce the *Quaternionic Laplacian* matrix, a positive semidefinite quaternion-valued Hermitian matrix which fully captures the directional and weight information of a digraph, even in the presence of digons, without restrictions on the sign or magnitude of the edge weights.

#### 3.1 The Quaternion Number System

Quaternions are an extension of complex numbers to three imaginary components [Hamilton, 1866]. They are often used in quantum mechanics, where they lead to elegant expressions of the Lorentz transformation, which forms the basis of modern relativity theory [Jia, 2008]. In computer graphics, quaternions are commonly used to represent and manipulate 3D objects for rotation estimation and pose graph optimization [Carlone et al., 2015].

Formally, a quaternion  $q \in \mathbb{H}$  takes the form  $q = q_0 + \mathbf{i}q_1 + \mathbf{j}q_2 + \mathbf{k}q_3$ , where  $q_0, q_1, q_2$  and  $q_3$  are real numbers and  $\mathbf{i}, \mathbf{j}$ , and  $\mathbf{k}$  are three imaginary units satisfying  $\mathbf{i}^2 = \mathbf{j}^2 = \mathbf{k}^2 = \mathbf{i}\mathbf{j}\mathbf{k} = -1$ . The four basis elements are  $1, \mathbf{i}, \mathbf{j}$ , and  $\mathbf{k}$ . The conjugate of  $q$  is  $\bar{q} \equiv q^* = q_0 - \mathbf{i}q_1 - \mathbf{j}q_2 - \mathbf{k}q_3$ .  $q$  is called imaginary if its real part  $q_0$  is zero. The multiplication of quaternions satisfies the distribution law but is not commutative. A quaternion-valued matrix  $Q = (q_{uv}) \in \mathbb{H}^{m \times n}$  reads  $Q = Q_0 + \mathbf{i}Q_1 + \mathbf{j}Q_2 + \mathbf{k}Q_3$ , with  $Q_0, Q_1, Q_2, Q_3 \in \mathbb{R}^{m \times n}$ .  $Q^\top = (q_{vu})$  is the transpose of  $Q$ .  $\bar{Q} = (\bar{q}_{uv})$  is the conjugate of  $Q$ .  $Q^* = (\bar{q}_{vu}) = \bar{Q}^\top$  is the conjugate transpose of  $Q$ . A square quaternion matrix  $Q \in \mathbb{H}^{n \times n}$  is called Hermitian if  $Q^* = Q$  and skew-Hermitian if  $Q^* = -Q$ . We denote the real part and the three imaginary parts of a quaternion  $q \in \mathbb{H}$  by  $\Re(q)$ ,  $\Im_1(q)$ ,  $\Im_2(q)$ , and  $\Im_3(q)$ .

#### 3.2 The Quaternionic Laplacian

Let us now introduce the Quaternionic Laplacian, which we denote by  $L^\vartheta$ . First, we introduce the following matrices:

- Let  $T := \text{sgn}(|A|) \in \{0, 1\}^{n \times n}$  be a binary matrix that encodes the graph's topology, with  $T_{uv} = 1$  if  $G$  contains an edge from node  $u$  to node  $v$  and  $T_{uv} = 0$  otherwise.
- Let  $O := T \odot T^\top \in \{0, 1\}^{n \times n}$  be the binary matrix that encodes the topology of the subgraph of  $G$  that only contains digons (by definition,  $O$  is symmetric and  $O_{uv} = O_{vu} = 1$  iff  $T_{uv} = T_{vu} = 1$ ).
- Let  $N := \text{sgn}(|A - A^\top|) \in \{0, 1\}^{n \times n}$  be a binary matrix that encodes the topology of the subgraph of  $G$  obtained by dropping any symmetric digons (by definition,  $N_{uv} = 0$  if  $A_{uv} = A_{vu}$  and  $N_{uv} = T_{uv}$  otherwise).
- Let  $R := \text{sgn}(|A| - |A^\top|) \in \{-1, 0, 1\}^{n \times n}$  be a signed binary matrix in which every asymmetric digon  $(u, v), (v, u)$  is reduced to a single edge in the direction of the largest absolute weight ( $R_{uv} = T_{uv}$  if  $A_{uv} > A_{vu}$ ,  $R_{uv} = -T_{uv}$  if  $A_{uv} < A_{vu}$ , and  $R_{uv} = 0$  otherwise).

With these definitions, we introduce the four matrices  $H^0, H^1, H^2, H^3$ , whose elements are valued in  $\{-1, 0, 1\}$ :

$$\begin{aligned} H^0 &:= ee^\top - N & H^1 &:= R \odot (ee^\top - O) \\ H^2 &:= O \odot N \odot (U(T) - L(T^\top)) & H^3 &:= -H^2, \end{aligned}$$

where  $U$  and  $L$  are the unary operators that construct an upper- or lower-triangular matrix from the upper or lower triangle of the matrix given to them as input.

$H^0$  only encodes  $G$ 's symmetric digons,  $H^1$  encodes all of  $G$ 's edges excluding digons, and  $H^2$  and  $H^3$  encode  $G$ 's asymmetric digons in a skew-symmetric way. We remark that the three matrices  $H^1, H^2, H^3$  are skew-symmetric by construction (i.e.,  $H_{uv}^1 = -H_{vu}^1, H_{uv}^2 = -H_{vu}^2, H_{uv}^3 = -H_{vu}^3$  for all  $u, v \in V$ ), whereas  $H^0$  is symmetric.

Based on the four matrices  $H^0, H^1, H^2, H^3$ , we now define the Quaternionic Laplacian as follows:

$$\begin{aligned} L^\vartheta &:= \bar{D}_s - H^\vartheta, \quad \text{with} \\ H^\vartheta &= A_s^1 \odot (H^0 + \mathbf{i}H^1) + \mathbf{j}A_s^2 \odot H^2 + \mathbf{k}A_s^3 \odot H^3, \end{aligned} \tag{1}$$

with  $A_s^1 := \frac{A+A^\top}{2}$ ,  $A_s^2 := \frac{U(A)+L(A^\top)}{2}$ ,  $A_s^3 := \frac{L(A)+U(A^\top)}{2}$ , and  $\bar{D}_s := \text{Diag}(|A_s^1|e)$ . Its normalized version reads:

$$L_{\text{norm}}^\vartheta := \bar{D}_s^{-\frac{1}{2}} L^\vartheta \bar{D}_s^{-\frac{1}{2}} = I - \bar{D}_s^{-\frac{1}{2}} H^\vartheta \bar{D}_s^{-\frac{1}{2}}. \quad (2)$$

### 3.3 On the Nature of the Elements of $H^\vartheta$

Let us illustrate how the topology of  $G$  and its weights are mapped into the matrix  $H^\vartheta$ .

1. For every edge  $(u, v) \in E$  with  $(v, u) \notin E$  (i.e., not contained in a digon)  $H_{uv}^\vartheta = -H_{vu}^\vartheta = 0 + \mathbf{i}\frac{1}{2}A_{uv} + \mathbf{j}0 + \mathbf{k}0$  holds. Thus, the edge is purely mapped in the first imaginary component ( $\mathbf{i}$ ) of  $H^\vartheta$ .
2. For every symmetric digon  $(u, v), (v, u) \in E$  with  $A_{uv} = A_{vu}$ ,  $H_{uv}^\vartheta = H_{vu}^\vartheta = \frac{1}{2}(A_{uv} + A_{vu}) + \mathbf{i}0 + \mathbf{j}0 + \mathbf{k}0$  holds. Thus, such digons are encoded purely in the real part of  $H^\vartheta$  (as if they coincided with an undirected edge).
3. For every asymmetric digon  $(u, v), (v, u) \in E$  with  $A_{uv} \neq A_{vu}$ ,  $H_{uv}^\vartheta = -H_{vu}^\vartheta = 0 + \mathbf{i}0 + \mathbf{j}\frac{1}{2}A_{uv} - \mathbf{k}\frac{1}{2}A_{vu}$  (if  $u < v$ ) and  $H_{uv}^\vartheta = -H_{vu}^\vartheta = 0 + \mathbf{i}0 - \mathbf{j}\frac{1}{2}A_{uv} + \mathbf{k}\frac{1}{2}A_{vu}$  (if  $u > v$ ) hold. Such digons are thus encoded purely in the second and third ( $\mathbf{j}$  and  $\mathbf{k}$ ) imaginary components.

$L^\vartheta$  realizes the same mapping as  $L^\sigma$  in cases 1 and 2, but not in case 3. In such a case, while in  $L^\sigma$  every asymmetric digon is mapped into a single directed edge in the direction of largest magnitude (thus losing parts of its topology), in  $L^\vartheta$  the topology of such a digon is completely preserved.

For each  $u, v \in V$ , the three imaginary parts of  $L^\vartheta$  are orthogonal: if  $u$  and  $v$  share only one edge, this edge is reported in the imaginary component  $\mathbf{i}$ ; if they share two edges of different weights, the two edges are reported in the imaginary components  $\mathbf{j}$  and  $\mathbf{k}$ ; if they share two edges of the same weight, the edges are reported as a single undirected edge in the real component of  $L^\vartheta$ ; if the two nodes share no edges, nothing is reported.

### 3.4 From a Graph to its Quaternionic Laplacian

As an illustrative example, consider the graph depicted in Figure 1, together with its weighted adjacency matrix. The graph has the following characteristics:

1. A single undirected edge  $(1, 2)$  (which is equivalent to a symmetric digon).
2. A directed edge  $(3, 1)$ .
3. Two asymmetric digons,  $(2, 4) - (4, 2)$  and  $(3, 4) - (4, 3)$ , with different weights that share the same sign.

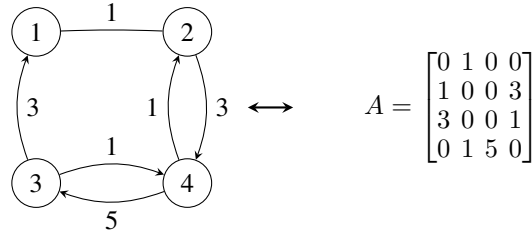


Figure 1: Graph and Adjacency Matrix

For this graph,  $L^\vartheta$  reads:

$$L^\vartheta := \bar{D}_s - H^\vartheta, \quad \text{with}$$

$$H^\vartheta := A_s^1 \odot (H^0 + \mathbf{i}H^1) + \mathbf{j}A_s^2 \odot H^2 + \mathbf{k}A_s^3 \odot H^3, \quad \text{and}$$

$$\text{with } A_s^1 = \begin{bmatrix} 0 & 1 & 1.5 & 0 \\ 1 & 0 & 0 & 2 \\ 1.5 & 0 & 0 & 3 \\ 0 & 2 & 3 & 0 \end{bmatrix}, A_s^2 = \begin{bmatrix} 0 & 0.5 & 0 & 0 \\ 0.5 & 0 & 0 & 1.5 \\ 0 & 0 & 0 & 0.5 \\ 0 & 1.5 & 0.5 & 0 \end{bmatrix}, A_s^3 = \begin{bmatrix} 0 & 0.5 & 1.5 & 0 \\ 0.5 & 0 & 0 & 0.5 \\ 1.5 & 0 & 0 & 2.5 \\ 0 & 0.5 & 2.5 & 0 \end{bmatrix},$$

$$H^0 = \begin{bmatrix} 1 & 1 & 0 & 1 \\ 1 & 1 & 1 & 0 \\ 0 & 1 & 1 & 0 \\ 1 & 0 & 0 & 1 \end{bmatrix}, \quad H^1 = \begin{bmatrix} 0 & -1 & 0 & 0 \\ 1 & 0 & 0 & 0 \\ 0 & 0 & 0 & 0 \\ 0 & 0 & 0 & 0 \end{bmatrix},$$

$$H^2 = \begin{bmatrix} 0 & 0 & 0 & 0 \\ 0 & 0 & 0 & 1 \\ 0 & 0 & 0 & 1 \\ 0 & -1 & -1 & 0 \end{bmatrix}, \quad H^3 = \begin{bmatrix} 0 & 0 & 0 & 0 \\ 0 & 0 & 0 & -1 \\ 0 & 0 & 0 & -1 \\ 0 & 1 & 1 & 0 \end{bmatrix}.$$

We note that  $H^0$  contains a 1 for each edge that does not belong to a digon with different weights or to a single directed edge without an antiparallel one. It features an all-1 diagonal, whose values would become zeros after the multiplication by  $A_s^1$ .  $H^1$  contains a  $\pm 1$  for each undirected edge with a positive sign for the actual edge direction and a negative one for the inverse direction.  $H^2$  and  $H^3$  contain a 1 for each pair of edges belonging to a digon with different edge weights. By construction,  $H^3$  is the opposite of  $H^2$ .

$L^\vartheta$  thus reads:

$$L^\vartheta = \begin{bmatrix} 2.5 & -1 & \mathbf{i} 1.5 & 0 \\ -1 & 3 & 0 & -\mathbf{j} 1.5 + \mathbf{k} 0.5 \\ -\mathbf{i} 1.5 & 0 & 4.5 & -\mathbf{j} 0.5 + \mathbf{k} 2.5 \\ 0 & \mathbf{j} 1.5 - \mathbf{k} 0.5 & \mathbf{j} 0.5 - \mathbf{k} 2.5 & 5 \end{bmatrix}.$$

By inspecting  $L^\vartheta$ , one can observe that it encodes the elements of the graph in the following way:

1. The undirected edge is encoded via the real component  $L_{12}^\vartheta = L_{21}^\vartheta = -1$ ;
2. The directed edge is encoded via the  $\mathbf{i}$  component,  $L_{13}^\vartheta = L_{31}^\vartheta = \mathbf{i} 1.5$ ;
3. The two digons with different weights that share the same sign are encoded via the  $\mathbf{j}$  and  $\mathbf{k}$  components:
  - (a)  $L_{24}^\vartheta = -L_{42}^\vartheta = -\mathbf{j} 1.5 + \mathbf{k} 0.5$ ;
  - (b)  $L_{34}^\vartheta = -L_{43}^\vartheta = -\mathbf{j} 0.5 + \mathbf{k} 2.5$ .

### 3.5 Relationship between $L^\vartheta$ and other Laplacians

The Quaternionic Laplacian is designed in such a way that it satisfies several desirable properties which we now illustrate.

For undirected graphs with positive edge weights,  $L^\vartheta$  generalizes the classical Laplacian  $L$ :

**Theorem 1.**  $L^\vartheta = L$  for every graph with  $A$  symmetric and nonnegative and  $D_{vv} > 0$  for all  $v \in V$ .

For digraphs with arbitrary edge weight featuring, if any, symmetric digons,  $L^\vartheta$  generalizes the Sign-Magnetic Laplacian  $L^\sigma$ :

**Theorem 2.**  $L^\vartheta = L^\sigma$  if, for all  $u, v \in V$ , either  $A_{uv} = 0$  or  $A_{uv} = A_{vu}$ .

As  $L^\sigma$  coincides with  $L^{(q)}$  with  $q = \frac{1}{4}$  [Fiorini et al., 2022], the following holds:

**Corollary 1.**  $L^\vartheta = L^{(q)}$  with  $q = \frac{1}{4}$  for every digraph with  $A \in \{0, 1\}^{n \times n}$  containing, if any, symmetric digons.

If the graph does not feature any symmetric digons, the matrix  $H^\vartheta$  from which  $L^\vartheta$  is defined coincides with a linear combination of  $L^\sigma$  with a Hermitian matrix encoding the asymmetric digons:

**Theorem 3.** Consider a weighted digraph without symmetric digons and let  $H^m := (A_s^2 \odot H_1^2 + A_s^3 \odot H_1^3)$ , where  $H_1^2 = N \odot (U(T) - L(T^\top))$  and  $H_1^3 = -H_1^2$ . We have  $H^0 = 0$  and  $H^\vartheta = H^\sigma \odot (ee^\top - O) + O \odot H^m$ . Thus, each component of  $H_{uv}^\vartheta$  is a linear combination of the component  $H_{uv}^\sigma$  of the Sign-Magnetic Laplacian  $H^\sigma$  and the component  $H_{uv}^m$  of the quaternionic Hermitian matrix  $H^m$ .

### 3.6 Spectral properties of $L^\vartheta$

As  $H^\vartheta$  is Hermitian by construction,  $L^\vartheta$  and  $L_{\text{norm}}^\vartheta$  are Hermitian as well. As any Hermitian quaternion matrix  $Q$  is diagonalizable via the (right) eigenvalue decomposition  $Q = U^* \Lambda U$  (see Qi and Luo [2021] for a proof),  $L^\vartheta$  and  $L_{\text{norm}}^\vartheta$  satisfy the property P.1. Both matrices admit exactly  $n$  right eigenvalue-eigenvector pairs, all of which are real:

**Theorem 4.**  $L^\vartheta$  and  $L_{\text{norm}}^\vartheta$  are positive semidefinite.

The right eigenvalues of the normalized version of  $L^\vartheta$  are upper bounded by 2:

**Theorem 5.**  $\lambda_{\max}(L_{\text{norm}}^\vartheta) \leq 2$ , where  $\lambda_{\max}$  denotes the (real) right eigenvalue of largest value.

These theorems show that  $L^\vartheta$  and  $L_{\text{norm}}^\vartheta$  enjoy the two remaining properties P.2 and P.3. Thus,  $L_{\text{norm}}^\vartheta$  can be employed for the definition of a convolution operator, as shown in the following section.

## 4 QuaterNet: a spectral GCN based on $L^\vartheta$

Following Hammond et al. [2011] and Kipf and Welling [2017], we define the convolution operation of a signal  $x \in \mathbb{R}^n$  and a filter  $y \in \mathbb{R}^n$  as

$$y * x = Yx = (\theta_0 I - \theta_0 (L_{\text{norm}}^\vartheta - I))x = \theta_0 (2I - L_{\text{norm}}^\vartheta)x. \quad (3)$$

The equation is obtained by approximating the Fourier transform on the graph Laplacian with Chebyshev's polynomial (of the first kind) of order 1.

Due to Theorems 4 and 5,  $L_{\text{norm}}^\vartheta$  enjoys properties P.1, P.2, and P.3. Thus,  $Y$  is a well-defined convolution operator and, by definition of  $L_{\text{norm}}^\vartheta$ , we have:

$$\begin{aligned} y * x = Yx &= \theta_0 (2I - (I - \bar{D}_s^{-\frac{1}{2}} H^\vartheta \bar{D}_s^{-\frac{1}{2}})x \\ &= \theta_0 (I + \bar{D}_s^{-\frac{1}{2}} H^\vartheta \bar{D}_s^{-\frac{1}{2}})x. \end{aligned} \quad (4)$$

Following Kipf and Welling [2017] to avoid numerical instabilities, we apply Eq. (4) with  $\tilde{D}_s^{-\frac{1}{2}} \tilde{H}^\vartheta \tilde{D}_s^{-\frac{1}{2}}$  rather than  $I + \bar{D}_s^{-\frac{1}{2}} H^\vartheta \bar{D}_s^{-\frac{1}{2}}$ , where  $\tilde{H}^\vartheta$  and  $\tilde{D}_s$  are defined as a function of  $\tilde{A} := A + I$  rather than  $A$ .

We generalize the feature vector signal  $x \in \mathbb{H}^{n \times 1}$  to a feature matrix signal  $X \in \mathbb{H}^{n \times c}$  with  $c$  input channels (i.e., a  $c$ -dimensional feature vector for every node of the graph). Let  $\Theta \in \mathbb{H}^{c \times f}$  be a matrix representing the parameters of an  $f$ -dimensional filter and let  $\phi$  be an activation function (such as the *ReLU*) applied component-wise to the input matrix.

In QuaterGCN, we define the convolutional layer as the following mapping from  $X$  to  $Z^\sigma(X) \in \mathbb{H}^{n \times f}$ :

$$Z^\vartheta(X) = \phi(\tilde{D}_s^{-\frac{1}{2}} \tilde{H}^\vartheta \tilde{D}_s^{-\frac{1}{2}} X \Theta) = \phi(X^\vartheta \Theta).$$

Since  $X^\vartheta \Theta$  is a quaternion-valued matrix and traditional activation functions require a real argument, we follow the approach of Parcollet et al. [2019] and apply the activation function  $\phi$  to each element of its quaternionic input as

$$\phi : (a + \mathbf{i}b + \mathbf{j}c + \mathbf{k}d) \mapsto \phi(a) + \mathbf{i}\phi(b) + \mathbf{j}\phi(c) + \mathbf{k}\phi(d).$$

Thanks to this, the output  $Z^\vartheta(X)$  of the convolutional layer is quaternion-valued. As usually done in spectral GCNs, we lastly adopt an *unwind* layer by which we transform the matrix  $Z^\vartheta(X) \in \mathbb{H}^{n \times f}$  into the 4-times larger real-valued matrix

$$(\Re(Z^\vartheta(X)) \mid \Im_1(Z^\vartheta(X)) \mid \Im_2(Z^\vartheta(X)) \mid \Im_3(Z^\vartheta(X))) \in \mathbb{R}^{n \times 4f}.$$

As stated by Parcollet et al. [2020] and Nguyen et al. [2021], the adoption of quaternion algebra in the product  $X^\vartheta \Theta$  leads to an extensive interaction among the components of  $X^\vartheta$  which is likely to lead to more expressive vector representations than those achieved with real- and complex-valued networks.

Based on the task at hand (see next section), after the convolution layer we described before QuaterGCN features either a linear layer with weights  $W$  or a 1D convolution. Considering, for example, a node-classification task of predicting which of a set of unknown classes a graph vertex belongs to, QuaterGCN implements the function

$$\text{softmax} \left( \text{unwind} \left( Z^{\vartheta(2)} \left( Z^{\vartheta(1)} \left( X^{(0)} \right) \right) W \right) \right),$$

where  $X^{(0)} \in \mathbb{H}^{n \times c}$  is the input feature matrix,  $Z^{\vartheta(1)} \in \mathbb{H}^{n \times f_1}$  and  $Z^{\vartheta(2)} \in \mathbb{H}^{n \times f_2}$  are two convolutional layers,  $W \in \mathbb{R}^{4f_2 \times d}$  are the weights of the linear layer (with  $d$  being the number of classes), and  $\text{softmax} : \mathbb{R}^{n \times d} \rightarrow [0, 1]^{n \times d}$  is the normalized exponential activation function typically used to recover the node classes.

### 4.1 Complexity of QuaterGCN

For a graph with  $n$  nodes with a  $c$ -dimensional feature vector each, the complexity of QuaterGCN, with two convolutional layers with  $f_1$  and  $f_2$  filters each, is  $O(nc(n + f_1) + nf_1(n + f_2) + m^{\text{train}} f_2 d)$  for an edge-classification task and  $O(nc(n + f_1) + nf_1(n + f_2) + nf_2 d)$  for a node-classification one, where  $d$  is the number of classes (see the next section for more details on these tasks). Such a complexity is quadratic in the number of nodes  $n$  and it coincides with MagNet's, MSGNN's, and SigMaNet's. As the scalar-scalar product between two quaternions requires 8 multiplications and 7 additions between real numbers rather than 4 multiplications and 3 additions for the complex case and a single multiplication for the real case, the least-efficient operation carried out by QuaterGCN can be up to 64 times slower than it would be if the network featured real-only numbers. While apparently large, such a quantity is constant w.r.t. the size of the graph, which implies that QuaterGCN scales comparably to previous proposals in the literature.

## 5 Numerical Experiments

We compare QuaterGCN with state-of-the-art GCNs across four tasks: *node classification* (NC), *three-class edge prediction* (3CEP), *four-class edge prediction* (4CEP), and *five-class edge prediction* (5CEP). Throughout this section, the tables report the best results in **boldface** and the second-best are underlined. The datasets and the code we used are publicly available at <https://github.com/Stefa1994/QuaterGCN>.

We experiment on the six widely-used real-world directed graphs Bitcoin-OTC, Bitcoin Alpha, WikiRfa, Telegram, Slashdot, and Epinions (see Kumar et al. [2016], Bovet and Grindrod [2020], West et al. [2014], Leskovec et al. [2010]). The first three feature edge weights of unrestricted sign and magnitude; the fourth contains graphs with positive edge weights, while the last two have graphs with weights satisfying  $A \in \{-1, 0, +1\}^{n \times n}$ .

To study the relationship between performance and graph density, we also employ DBSM graphs: synthetic digraphs with positive random weights already used by Fiorini et al. [2022]. They are generated via a direct stochastic block model (DSBM) with edge weights greater than 1 and a different number of nodes per cluster ( $N$ ) and number of clusters ( $C$ ). Inter- and intra-cluster edges are created with, respectively, probability  $\alpha_{uv}$  and  $\alpha_{uu}$ , and a connected pair of nodes  $\{u, v\}$  with  $u < v$  shares the edge  $(u, v)$  with probability  $\beta_{uv}$  and  $(v, u)$  with probability  $1 - \beta_{uv}$ .

As the DBSM graphs are digons-free, we introduce a second class of synthetic digraphs with a variable percentage of digons  $\delta \in (0, 1)$  with positive random weights between 2 and 4: Di150 (150 nodes) and Di500 (500 nodes). Di150 features graphs with  $N = 150$ ,  $C = 5$ ,  $\alpha_{uu} = 0.1$ ,  $\beta_{uv} = 0.2$ , and  $\alpha_{uv} = 0.6$ . Di500 contains graphs with  $N = 500$ ,  $C = 5$ ,  $\alpha_{uu} = 0.1$ ,  $\beta_{uv} = 0.2$ , and  $\alpha_{uv} = 0.1$ . Notice that Di500 is sparser than Di250.

Table 2: Accuracy (%) on the node classification task

	Node classification						
	DBSM				Di500		
	Telegram	$\alpha_{uv} = 0.05$	$\alpha_{uv} = 0.08$	$\alpha_{uv} = 0.1$	$\delta = 0.2$	$\delta = 0.5$	$\delta = 0.7$
ChebNet	61.73±4.25	20.06±00.18	20.50±00.77	19.98±00.06	19.90±0.24	20.00±0.00	19.94±0.13
GCN	60.77±3.67	20.06±00.18	20.02±00.06	20.01±00.01	20.04±0.12	20.10±0.30	20.08±0.30
QGNN	51.35±9.10	20.03±00.12	20.01±00.02	19.99±00.07	20.23±0.21	19.94±0.18	20.00±0.00
APPNP	55.19±6.26	33.46±07.43	34.72±14.98	36.16±14.92	20.64±1.32	20.16±0.37	20.10±0.30
SAGE	65.38±5.15	67.64±09.81	68.28±10.92	82.96±10.98	23.68±3.83	20.44±0.95	20.02±0.14
GIN	72.69±4.62	28.46±08.01	20.12±00.20	20.98±08.28	20.14±0.42	19.88±0.36	20.00±0.00
GAT	72.31±3.01	22.34±03.13	21.90±02.89	21.58±01.80	19.90±0.20	20.04±0.28	20.16±0.42
SSSNET	24.04±9.29	<b>91.04±03.60</b>	94.94±01.01	96.77±00.80	31.41±5.91	22.34±1.31	<u>21.13±1.03</u>
DGCN	71.15±6.32	30.02±06.57	30.22±11.94	28.40±08.62	20.10±0.30	20.00±0.00	20.00±0.00
DiGraph	71.16±5.57	53.84±14.28	38.50±12.20	34.78±09.94	<u>32.82±2.14</u>	<u>24.44±2.33</u>	20.76±1.34
DiGCL	64.62±4.50	19.51±01.21	20.24±00.84	19.98±00.45	20.00±0.00	20.00±0.00	20.00±0.00
MagNet	55.96±3.59	78.64±01.29	87.52±01.30	91.58±01.04	31.46±2.20	22.74±1.12	20.88±1.62
SigMaNet	<u>74.23±5.24</u>	87.44±00.99	<u>96.14±00.64</u>	<u>98.60±00.31</u>	31.26±2.08	22.32±1.69	19.94±1.07
GraQuaterGCN	<b>75.58±3.85</b>	<u>87.46±00.73</u>	<b>96.44±00.12</b>	<b>98.80±00.20</b>	<b>64.28±1.04</b>	<b>70.60±1.62</b>	<b>71.58±1.52</b>

### 5.1 Node Classification Task (NC)

The task is to predict the class of each node. We consider the Telegram dataset and the 9 aforementioned synthetic datasets, i.e., every dataset except for those that lack a pre-determined node class.

We compare QuaterGCN with: (i) the three spectral GCNs designed for undirected graphs: ChebNet [Defferrard et al., 2016] and GCN [Kipf and Welling, 2017] and the spectral GCN with quaternionic weights QGNN designed for undirected graphs [Nguyen et al., 2021]; (ii) the four spectral GCNs designed for directed graphs: DGCN [Tong et al., 2020a], DiGraph [Tong et al., 2020b], DiGCL [Tong et al., 2021], MagNet [Zhang et al., 2021a], and SigMaNet [Fiorini et al., 2022]; and (iii) the five spatial GCNs: APPNP [Klicpera et al., 2019], SAGE [Hamilton et al., 2017], GIN [Xu et al., 2018], GAT [Veličković et al., 2018], and SSSNET [He et al., 2022c]. The experiments are run with 10-fold cross-validation with a 60%/20%/20% split for training, validation, and testing.

Table 2 and 3 show that QuaterGCN achieves a remarkable performance across all datasets, being the best method in 9 cases out of 10. The percentage difference between QuaterGCN and the second-best performer ranges from 0.2% (for DBSM with  $\alpha_{uv} = 0.1$ ) to 242.81% (for Di500 with  $\delta = 0.7$ ). The average performance improvement of QuaterGCN across all datasets is 68.27%. QuaterGCN consistently outperforms the state of the art on, in particular, Di500 and Di150, where it achieves an average improvement w.r.t. the second-best performer of 28.19% on the Di150 dataset and



Table 3: Accuracy (%) on the node classification task

	Node classification		
	Di150		
	$\delta = 0.2$	$\delta = 0.5$	$\delta = 0.7$
ChebNet	19.93±00.20	20.00±00.00	20.00±00.00
GCN	20.00±00.00	20.00±00.00	20.07±00.20
QGNN	19.87±00.40	19.93±00.20	20.00±00.00
APPNP	22.87±08.60	21.07±03.20	20.00±00.00
SAGE	78.40±14.35	33.20±14.10	20.33±01.69
GIN	24.67±06.76	28.13±08.87	23.67±06.24
GAT	51.20±10.18	29.33±10.05	21.40±03.78
SSSNET	92.71±12.48	86.18±17.77	61.78±24.44
DGCN	26.87±08.43	21.87±05.60	20.00±00.00
DiGraph	97.40±01.01	88.27±03.14	58.93±08.47
DiGCL	20.00±00.00	20.00±00.00	20.00±00.00
MagNet	97.87±01.90	74.53±10.43	31.13±06.65
SigMaNet	74.67±04.15	49.60±03.07	24.67±04.40
QuaterGCN	<b>99.73±00.33</b>	<b>99.85±00.13</b>	<b>99.93±00.03</b>

Table 4: Accuracy (%) on the three-class edge prediction task

	Three-Class Edge prediction								
	Di150						DBSM		
	Telegram	Bit Alpha*	Bitcoin OTC*	$\delta = 0.2$	$\delta = 0.5$	$\delta = 0.7$	$\alpha_{uv} = 0.05$	$\alpha_{uv} = 0.08$	$\alpha_{uv} = 0.1$
ChebNet	63.65±4.65	82.82±0.82	83.01±1.09	40.58±0.07	48.81±0.53	52.10±0.88	33.34±0.01	33.36±0.07	33.33±0.02
GCN	53.86±1.60	82.61±0.67	82.49±0.99	40.60±0.07	49.00±0.08	<b>53.51±0.10</b>	33.33±0.02	33.32±0.03	33.34±0.01
QGNN	52.33±1.50	80.93±0.63	79.97±0.80	40.60±0.07	<u>49.00±0.08</u>	52.51±0.09	33.38±0.09	33.43±0.26	33.37±0.04
APPNP	50.82±6.31	82.14±0.89	81.77±0.63	40.55±0.08	48.98±0.09	52.50±0.10	37.67±4.04	37.84±5.70	37.52±5.33
SAGE	69.28±7.24	55.82±1.60	85.19±0.64	40.62±0.14	49.00±0.08	52.52±0.09	39.50±3.74	38.51±3.55	42.69±3.87
GIN	58.41±1.26	77.93±0.86	76.35±0.77	40.56±0.08	48.98±0.10	52.47±0.10	34.65±2.62	33.34±0.01	33.52±0.37
GAT	67.34±2.50	84.93±1.20	85.02±0.74	40.64±1.79	48.44±1.63	52.51±0.09	33.70±0.79	33.35±0.07	33.91±1.63
DGCN	75.01±3.60	85.01±0.95	85.03±0.64	40.57±0.06	48.82±0.50	52.51±0.08	34.12±2.17	34.78±2.11	35.24±2.36
DiGraph	74.27±1.02	83.66±0.72	84.14±0.82	41.38±0.92	48.90±0.11	52.40±0.09	41.30±1.41	42.57±1.62	53.57±1.73
DiGCL	66.03±0.84	77.68±0.74	76.35±0.77	29.70±0.04	25.50±0.04	23.74±0.04	38.30±0.15	38.17±0.07	37.58±0.12
MagNet	<b>82.28±0.84</b>	85.72±0.67	85.66±0.78	45.47±1.70	48.78±0.35	52.19±0.43	43.62±1.11	46.76±1.13	47.76±1.12
SigMaNet	80.13±0.87	85.52±0.61	84.61±0.79	<u>45.50±1.41</u>	47.02±0.91	51.81±0.80	<u>43.65±0.36</u>	<b>47.26±0.17</b>	<u>48.60±0.17</u>
QuaterGCN	<u>81.17±0.74</u>	<b>86.17±0.57</b>	<b>86.06±0.60</b>	<b>47.14±0.21</b>	<b>49.01±0.16</b>	52.07±0.22	<b>44.10±0.58</b>	<b>47.26±0.56</b>	<b>48.68±0.26</b>

Table 5: Accuracy (%) on the four-class edge prediction tasks

	Four-Class Edge prediction				
	Bitcoin Alpha	Bitcoin OTC	WikiRfa	Slashdot	Epinions
SGCN	48.05±0.29	52.52±0.71	68.37±0.51	64.01±0.24	67.99±0.56
SiGAT	50.12±1.80	50.86±1.45	57.68±0.63	54.82±0.32	60.21±0.26
SDGNN	48.05±0.29	54.77±0.67	62.35±1.09	62.82±4.16	69.48±0.13
SNEA	47.61±1.26	49.25±0.86	59.30±1.32	57.66±0.24	60.35±0.45
SSSNET	49.53±1.13	52.75±1.71	65.84±0.77	64.53±1.98	69.89±2.26
SigMaNet	59.59±1.68	60.79±0.82	74.09±0.14	78.54±0.17	79.12±0.22
MSGNN	58.91±1.17	<u>63.12±0.86</u>	<u>75.07±0.41</u>	<b>79.46±0.25</b>	<u>80.96±0.32</u>
QuaterGCN	<b>61.74±0.94</b>	<b>65.36±0.84</b>	<b>75.19±0.47</b>	<u>79.21±0.13</u>	<b>81.10±0.18</b>

of 175% on the Di500 one. The larger improvement of QuaterGCN and, in particular, the overall weaker performance of every other method on the Di500 dataset seems to be correlated with the dataset being sparser than the smaller Di150, which suggests that the learning task is harder. The difference between QuaterGCN and QGNN (the only available GCN with quaternion-valued weights which, though, employs the classical real-valued Laplacian), is substantial, as QuaterGCN outperforms QGNN by 309% on average. As the two networks share a similar architecture, we attribute such a large difference to QuaterGCN’s convolution being done via our proposed Quaternionic Laplacian  $L^q$ .

Table 6: Accuracy (%) on the five-class edge prediction tasks

	Five-Class Edge prediction				
	Bitcoin Alpha	Bitcoin OTC	WikiRfa	Slashdot	Epinions
SGCN	78.43±0.36	77.54±0.56	67.74±0.29	64.74±0.16	74.07±0.32
SiGAT	76.68±0.47	74.37±1.18	58.49±1.51	48.01±0.95	57.58±1.34
SDGNN	77.75±0.82	77.28±0.58	62.83±1.90	60.53±4.88	73.27±0.09
SNEA	79.25±0.38	77.36±0.27	62.61±0.44	62.21±0.16	70.70±0.31
SSSNET	77.89±0.41	75.06±0.55	63.74±2.58	67.15±0.44	73.40±1.16
SigMaNet	81.68±0.37	80.92±0.36	74.22±0.12	78.31±0.06	82.85±0.08
MSGNN	<u>81.95±0.47</u>	<u>82.02±0.13</u>	<b>76.63±0.24</b>	<u>78.45±0.35</u>	<u>83.54±0.23</u>
QuaterGCN	<b>82.56±0.46</b>	<b>82.13±0.21</b>	<u>76.33±0.16</u>	<b>78.55±0.35</b>	<b>84.03±0.09</b>

### 5.2 Three-Class Edge Prediction Task (3CEP)

The task is to predict whether  $(u, v) \in E$ ,  $(v, u) \in E$ , or  $(u, v) \notin E \wedge (v, u) \notin E$ . In order to maximize the number of spectral methods we can compare to, for this task our analysis focuses on the datasets with positive weights, i.e., Telegram, DSBM, Di150, and D500. Following Fiorini et al. [2022], we also consider Bitcoin Alpha\* and Bitcoin OTC\*, obtained by removing any negative-weight edge from Bitcoin Alpha and Bitcoin OTC.

We compare QuaterGCN to the same methods we considered for the NC task. We run the experiments with 10-fold cross-validation with an 80%/15%/5% split for training, testing, and validation, preserving graph connectivity.

The results are reported in Table 4. Those obtained on the Di500 dataset are omitted as on it every method achieves the same performance of about 30% (equal to a uniform random predictor). The table shows that QuaterGCN outperforms the other methods on 7 datasets out of 9. Compared with the second-best model, QuaterGCN achieves an average performance improvement of 0.98%, with a maximum of 3.60% and a minimum of 0.02%.

Differently from the NC task, in the 3CEP task the difference in performance between the methods is smaller, as already observed by Zhang et al. [2021a] and Fiorini et al. [2022]. Nevertheless, the results indicate that the advantages provided by the Quaternionic Laplacian are still event, albeit being of smaller magnitude.

Focusing on QGNN, QuaterGCN outperforms it on 9 out of 10 datasets by an average of 25.58%. This further reinforces that the better performance of QuaterGCN is largely due to it relying on our proposed Laplacian matrix  $L^q$  rather than on the mere adoption of quaternionic weights as done in QGNN with the classical Laplacian.

Table 4 suggests that simpler methods designed for undirected graphs perform increasingly better when  $\delta$  increases on the Di150 dataset. This is likely due the fact that these graphs feature a small difference in edge weight. If  $A_{uv} \simeq A_{vu}$ , not much is lost if the (almost symmetric) digon  $(u, v), (v, u)$  is reduced to a single undirected edge of weight  $\frac{1}{2}(A_{uv} + A_{vu})$ , as done when, e.g., using the classical real-valued Laplacian matrix, as this would only lead to a small loss of information, if any. What is more, the larger the number of digons, the more the graph becomes close to being undirected if the difference in weight is small, which explains why simpler (and arguably easier to train) methods designed for undirected graphs achieve an increasingly better performance as the percentage of digons  $\delta$  increases.

### 5.3 Four/Five-Class Edge Prediction Task (4/5CEP)

The 4CEP task is to predict whether  $(u, v) \in E^+$ ,  $(u, v) \in E^-$ ,  $(v, u) \in E^+$ , and  $(v, u) \in E^-$  (with  $E^+$  and  $E^-$  being the positive- and negative-weight edges), while the 5CEP task also considers the class where  $(u, v) \notin E \wedge (v, u) \notin E$ . Due to their nature, for both tasks we focus on every dataset featuring both positive and negative weights, i.e., on all the real-world datasets except for Telegram. We run the experiments with 5-fold cross-validation with an 80%/20% split for training and testing, preserving graph connectivity.

Due to the nature of the tasks, we compare QuaterGCN against the only methods that can handle the sign of the edge weights, i.e.: *i*) the signed graph neural networks SGCN [Derr et al., 2018], SiGAT [Huang et al., 2019], SNEA Li et al. [2020], SDGNN [Huang et al., 2021], and SSSNET [He et al., 2022c]; and *ii*) the spectral GCNs that are well-defined for negative edge weights, i.e., SigMaNet [Fiorini et al., 2022] and MSGNN He et al. [2022b].

Table 5 and 6 show that, when compared to the other approaches, QuaterGCN achieves superior performance in 8 out of 10 cases, while being the second-best model in the other 2. In comparison with the second-best model, QuaterGCN achieves an average performance improvement of 1.14%, with a maximum of 3.61% and a minimum of 0.13%.

While not as large as for the NC task, the better performance that QuaterGCN achieves on the 4CEP and 5CEP tasks confirms the superior performance of the model we proposed.

## 6 Conclusions

We have proposed the *Quaternionic Laplacian*  $L^q$ , a quaternion-valued graph Laplacian which generalizes different previously-proposed Laplacian matrices while allowing for the seamless representation of graphs and digraphs of any weight and sign featuring any number of digons without suffering from losses of topological information. We have then proposed QuaterGCN, a spectral GCN with quaternionic network weights that employs a quaternion-valued convolution operator built on top of  $L^q$ . Our extensive experimental campaign has highlighted the advantages of employing our quaternion-valued graph Laplacian matrix to leverage the full topology of input graphs featuring digons. Future works include extending the Quaternionic Laplacian to multi-relational graphs with multiple directional edges and to temporal (time-extended) graphs.

## Acknowledgements

This work was partially funded by the PRIN 2020 project *ULTRA OPTYMAL - Urban Logistics and sustainable TRAnspotation: OPTimization under uncertainty and MACHine Learning* (grant number 20207C8T9M) and the PRIN-PNRR 2022 project *HEXAGON: Highly-specialized EXact Algorithms for Grid Operations at the National level* (grant number P20227CYT3), both funded by the Italian University and Research Ministry.

## References

- Ashish Vaswani, Noam Shazeer, Niki Parmar, Jakob Uszkoreit, Llion Jones, Aidan N Gomez, Łukasz Kaiser, and Illia Polosukhin. Attention is all you need. In I. Guyon, U. V. Luxburg, S. Bengio, H. Wallach, R. Fergus, S. Vishwanathan, and R. Garnett, editors, *Advances in Neural Information Processing Systems*, volume 30. Curran Associates, Inc., 2017.
- Waqar Ahmed Khan, Sai Ho Chung, Muhammad Usman Awan, and Xin Wen. Machine learning facilitated business intelligence (part i) neural networks learning algorithms and applications. *Industrial Management & Data Systems*, 120(1):164–195, 2020.
- Priyanka Dixit and Sanjay Silakari. Deep learning algorithms for cybersecurity applications: A technological and status review. *Computer Science Review*, 39:100317, 2021.
- Michael M Bronstein, Joan Bruna, Yann LeCun, Arthur Szlam, and Pierre Vandergheynst. Geometric deep learning: going beyond euclidean data. *IEEE Signal Processing Magazine*, 34(4):18–42, 2017.
- Zi Ye, Yogan Jaya Kumar, Goh Ong Sing, Fengyan Song, and Junsong Wang. A comprehensive survey of graph neural networks for knowledge graphs. *IEEE Access*, 10:75729–75741, 2022. doi: 10.1109/ACCESS.2022.3191784.
- Keyulu Xu, Weihua Hu, Jure Leskovec, and Stefanie Jegelka. How powerful are graph neural networks? *arXiv preprint arXiv:1810.00826*, 2018.
- Petar Veličković, Guillem Cucurull, Arantxa Casanova, Adriana Romero, Pietro Liò, and Yoshua Bengio. Graph attention networks. In *International Conference on Learning Representations*, 2018.
- Yujia Li, Richard Zemel, Marc Brockschmidt, and Daniel Tarlow. Gated graph sequence neural networks. In *Proceedings of ICLR’16*, April 2016.
- Thomas. N. Kipf and Max Welling. Semi-supervised classification with graph convolutional networks. In *5th International Conference on Learning Representations, ICLR 2017 - Conference Track Proceedings*, 2017.
- Yixuan He, Xitong Zhang, Junjie Huang, Benedek Rozemberczki, Mihai Cucuringu, and Gesine Reinert. PyTorch Geometric Signed Directed: A Software Package on Graph Neural Networks for Signed and Directed Graphs. *arXiv preprint arXiv:2202.10793*, 2022a.
- Longcan Wu, Daling Wang, Shi Feng, Xiangmin Zhou, Yifei Zhang, and Ge Yu. Graph collaborative filtering for recommendation in complex and quaternion spaces. In *Proc. of Web Information Systems Engineering (WISE 2022): 23rd International Conference*, pages 579–594. Springer, 2022.
- Xitong Zhang, Yixuan He, Nathan Brugnone, Michael Perlmutter, and Matthew Hirn. Magnet: A neural network for directed graphs, 2021a.
- Stefano Fiorini, Stefano Coniglio, Michele Ciavotta, and Enza Messina. Sigmanet: One laplacian to rule them all. *arXiv preprint arXiv:2205.13459*, 2022.
- Elliott H Lieb and Michael Loss. Fluxes, Laplacians, and Kasteleyn’s theorem. In *Statistical Mechanics*, pages 457–483. Springer, 1993.
- Yixuan He, Michael Perlmutter, Gesine Reinert, and Mihai Cucuringu. Msgnn: A spectral graph neural network based on a novel magnetic signed laplacian. In *Learning on Graphs Conference*, pages 40–1. PMLR, 2022b.
- Taewook Ko. A graph convolution for signed directed graphs. *arXiv preprint arXiv:2208.11511*, 2022.
- Tu Dinh Nguyen, Dinh Phung, et al. Quaternion graph neural networks. In *Asian conference on machine learning*, pages 236–251. PMLR, 2021.
- Chenyu Wang, Lingxiao Li, Haiyang Zhang, and Dun Li. Quaternion-based knowledge graph neural network for social recommendation. *Knowledge-Based Systems*, 257:109940, 2022.
- Thanh Le, Huy Tran, and Bac Le. Knowledge graph embedding with the special orthogonal group in quaternion space for link prediction. *Knowledge-Based Systems*, page 110400, 2023.
- Jie Zhang, Bo Hui, Po-Wei Harn, Min-Te Sun, and Wei-Shinn Ku. smgc: A complex-valued graph convolutional network via magnetic laplacian for directed graphs, 2021b.
- Michaël Fanuel, Carlos M. Alaíz, and Johan A. K. Suykens. Magnetic eigenmaps for community detection in directed networks. *Physical Review E*, 95(2), Feb 2017. ISSN 2470-0053.
- William Rowan Hamilton. *Elements of quaternions*. Longmans, Green, & Company, 1866.
- Yan-Bin Jia. Quaternions and rotations. *Com S*, 477(577):15, 2008.

- Luca Carlone, Roberto Tron, Kostas Daniilidis, and Frank Dellaert. Initialization techniques for 3d slam: A survey on rotation estimation and its use in pose graph optimization. In *2015 IEEE international conference on robotics and automation (ICRA)*, pages 4597–4604. IEEE, 2015.
- Liquan Qi and Ziyang Luo. A note on quaternion skew-symmetric matrices. *arXiv preprint arXiv:2110.09282*, 2021.
- David K Hammond, Pierre Vandergheynst, and Rémi Gribonval. Wavelets on graphs via spectral graph theory. *Applied and Computational Harmonic Analysis*, 30(2):129–150, 2011.
- Titouan Parcollet, Mirco Ravanelli, Mohamed Morchid, Georges Linarès, Chiheb Trabelsi, Renato De Mori, and Yoshua Bengio. Quaternion recurrent neural networks. In *International Conference on Learning Representations*, 2019.
- Titouan Parcollet, Mohamed Morchid, and Georges Linarès. A survey of quaternion neural networks. *Artificial Intelligence Review*, 53:2957–2982, 2020.
- Srijan Kumar, Francesca Spezzano, V. S. Subrahmanian, and Christos Faloutsos. Edge weight prediction in weighted signed networks. In *2016 IEEE 16th International Conference on Data Mining (ICDM)*, pages 221–230, 2016. doi: 10.1109/ICDM.2016.0033.
- Alexandre Bovet and Peter Grindrod. The activity of the far right on Telegram. *ResearchGate preprint*, DOI: 10.13140/RG.2.2.16700.05764:1–19, 2020.
- Robert West, Hristo S Paskov, Jure Leskovec, and Christopher Potts. Exploiting social network structure for person-to-person sentiment analysis. *Transactions of the Association for Computational Linguistics*, 2:297–310, 2014.
- Jure Leskovec, Daniel Huttenlocher, and Jon Kleinberg. Signed networks in social media. In *Proceedings of the SIGCHI conference on human factors in computing systems*, pages 1361–1370, 2010.
- Michaël Defferrard, Xavier Bresson, and Pierre Vandergheynst. Convolutional neural networks on graphs with fast localized spectral filtering. *Advances in neural information processing systems*, 29, 2016.
- Zekun Tong, Yuxuan Liang, Changsheng Sun, David S. Rosenblum, and Andrew Lim. Directed graph convolutional network, 2020a.
- Zekun Tong, Yuxuan Liang, Changsheng Sun, Xinke Li, David S. Rosenblum, and Andrew Lim. Digraph inception convolutional networks. *Advances in Neural Information Processing Systems*, 2020-December(NeurIPS):1–12, 2020b. ISSN 10495258.
- Zekun Tong, Yuxuan Liang, Henghui Ding, Yongxing Dai, Xinke Li, and Changhu Wang. Directed graph contrastive learning. *Advances in Neural Information Processing Systems*, 34:19580–19593, 2021.
- Johannes Klicpera, Aleksandar Bojchevski, and Stephan Günnemann. Predict then propagate: Graph neural networks meet personalized pagerank. In *Proceedings of the 7th International Conference on Learning Representations*, pages 1–15, 2019.
- Will Hamilton, Zhitaoying, and Jure Leskovec. Inductive representation learning on large graphs. *Advances in neural information processing systems*, 30:1–11, 2017.
- Yixuan He, Gesine Reinert, Songchao Wang, and Mihai Cucuringu. Sssnet: Semi-supervised signed network clustering. In *Proceedings of the 2022 SIAM International Conference on Data Mining (SDM)*, pages 244–252. SIAM, 2022c.
- Tyler Derr, Yao Ma, and Jiliang Tang. Signed graph convolutional networks. In *2018 IEEE International Conference on Data Mining (ICDM)*, pages 929–934. IEEE, 2018.
- Junjie Huang, Huawei Shen, Liang Hou, and Xueqi Cheng. Signed graph attention networks. In *International Conference on Artificial Neural Networks*, pages 566–577. Springer, 2019.
- Yu Li, Yuan Tian, Jiawei Zhang, and Yi Chang. Learning signed network embedding via graph attention. In *Proceedings of the AAAI conference on artificial intelligence*, volume 34, pages 4772–4779, 2020.
- Junjie Huang, Huawei Shen, Liang Hou, and Xueqi Cheng. Sdgnn: Learning node representation for signed directed networks. 35:196–203, May 2021. URL <https://ojs.aaai.org/index.php/AAAI/article/view/16093>.

## A Code Repository and Licensing

The code written for this research work (which, in particular, implements QuaterGCN) is available at <https://anonymous.4open.science/r/QuaterGCN> and freely distributed under the Apache 2.0 license.<sup>2</sup>

The datasets (except for WikiRfa) and some code components were obtained from the PyTorch Geometric Signed Directed [He et al., 2022a] library (provided under the MIT license). The WikiRfa dataset is available at [https://networks.skewed.de/net/wiki\\_rfa](https://networks.skewed.de/net/wiki_rfa) under the BSD licence.<sup>3</sup> The methods used for the experimental analysis are available at <https://github.com/stefa1994/sigmanet> under the MIT license.<sup>4</sup>

## B Properties of the Quaternionic Laplacian

This section contains the proofs of the theorems reported in the main paper.

**Theorem 1.**  $L^\vartheta = L$  for every graph  $G$  with  $A$  symmetric and nonnegative and  $D_{vv} > 0$  for all  $v \in V$ .

*Proof.* As  $G$  is undirected, its adjacency matrix  $A$  is symmetric. Since, for such any such graph,  $W^D = 0$  and  $N^D = 0$  hold, we deduce  $H^\vartheta = H^0$ . This implies  $L^\vartheta = L$ , from which the claim follows.  $\square$

**Theorem 2.**  $L^\vartheta = L^\sigma$  if, for all  $u, v \in V$ , either  $A_{uv} = 0$ , or  $A_{uv} = A_{vu}$ .

*Proof.* Given a weighted directed graph, for each  $u, v \in V$ , if  $A_{uv} \neq 0$  and  $A_{vu} = 0$ , we have  $H_{uv}^\sigma = -H_{uv}^\vartheta = 0 + \mathbf{i}\frac{1}{2} = H_{uv}^\vartheta = -H_{vu}^\vartheta = 0 + \mathbf{i}\frac{1}{2} + \mathbf{j}0 + \mathbf{k}0$ ; if  $A_{uv} = A_{vu} = a$ , with  $a$  being some nonnegative real value, we have  $H_{uv}^\sigma = H_{uv}^\vartheta = 1 + \mathbf{i}0 = H_{uv}^\vartheta = H_{vu}^\vartheta = 1 + \mathbf{i}0 + \mathbf{j}0 + \mathbf{k}0$ . Thus, since  $H^\vartheta = H^\sigma$ , we have  $L^\vartheta = L^\sigma$  and the claim follows.  $\square$

**Theorem 3.** Consider a weighted digraph without symmetric digons and let  $H^m := (A_s^2 \odot H_1^2 + A_s^3 \odot H_1^3)$ , where  $H_1^2 = N \odot (U(T) - L(T^\top))$  and  $H_1^3 = -H_1^2$ . We have  $H^0 = 0$  and  $H^\vartheta = H^\sigma \odot (ee^\top - O) + O \odot H^m$ . Thus, each component of  $H_{uv}^\vartheta$  is a linear combination of the component  $H_{uv}^\sigma$  of the Sign-Magnetic Laplacian  $H^\sigma$  and of the components  $H_{uv}^m$  of the quaternionic Hermitian matrix  $H^m$ .

In the statement, the matrix  $H^m$  coincides, by construction, with the imaginary parts  $\Im_2(H^\vartheta)$  and  $\Im_3(H^\vartheta)$  of the matrix  $H^\vartheta$  and, therefore, encodes all the digons of the graph that do not have equal weights.

*Proof.* Given a weighted digraph without any digons of equal weight,  $H^\vartheta = A_s^1 \odot H^0 + \mathbf{i}A_s^1 \odot H^1 + \mathbf{j}A_s^2 \odot H^2 + \mathbf{k}A_s^3 \odot H^3$ , with  $H^0 = 0$  due to the nature of the graph under consideration. Collecting the first term of  $H^\vartheta$  by  $(ee^\top - O^D)$  shows that it coincides with  $H^\sigma \odot (ee^\top - O^D)$ . Collecting the second two terms by  $O^D$  shows that they coincide with  $(H^m \odot O^D)$ . This concludes the proof.  $\square$

<sup>2</sup><https://www.apache.org/licenses/LICENSE-2.0>

<sup>3</sup><https://choosealicense.com/licenses/bsd-2-clause/>

<sup>4</sup><https://choosealicense.com/licenses/mit/>

**Theorem 4.**  $L^\vartheta$  and  $L_{\text{norm}}^\vartheta$  are positive semidefinite.

*Proof.* By definition of  $L^\vartheta$ , we have  $\Re(L^\vartheta) = \bar{D}_s - A_s^1 \odot H^0$ ,  $\Im_1(L^\vartheta) = -A_s^1 \odot H^1$ ,  $\Im_2(L^\vartheta) = -A_s^2 \odot H^2$  and  $\Im_3(L^\vartheta) = -A_s^3 \odot H^3$ . By construction,  $\Re(L^\vartheta)$  is symmetric and  $\Im_1(L^\vartheta)$ ,  $\Im_2(L^\vartheta)$ , and  $\Im_3(L^\vartheta)$  are skew symmetric. It follows that  $L^\vartheta$  is a Hermitian matrix, which implies that  $x^* \Im_1(L^\vartheta) x = 0$ ,  $x^* \Im_2(L^\vartheta) x = 0$  and  $x^* \Im_3(L^\vartheta) x = 0$  hold for all  $x \in \mathbb{H}^n$ . As, by construction,  $\bar{D}_s = \text{Diag}(|A_s^1|e)$  and  $A_s^1$  is symmetric, we can show that  $x^* \Re(L^\vartheta) x \geq 0$  holds for all  $x \in \mathbb{H}^n$  via the following derivation:

$$2x^* \Re(L^\vartheta) x$$

$$\begin{aligned} &= 2 \sum_{u,v=1}^n (\bar{D}_s)_{uv} x_u x_v^* - 2 \sum_{u,v=1}^n (A_s^1)_{uv} x_u x_v^* (1 - H_{uv}^0) \\ &= 2 \sum_{u,v=1}^n (\bar{D}_s)_{uv} x_u x_v^* - 2 \sum_{u,v=1}^n (A_s^1)_{uv} x_u x_v^* (1 - \text{sgn}(|A_{uv} - A_{vu}|)) \\ &= 2 \sum_{u,v=1}^n (\bar{D}_s)_{uu} x_u x_u^* - 2 \sum_{u,v=1}^n (A_s^1)_{uv} x_u x_v^* (1 - \text{sgn}(|A_{uv} - A_{vu}|)) \\ &= 2 \sum_{u,v=1}^n |(A_s^1)_{uv}| |x_u|^2 - 2 \sum_{u,v=1}^n (A_s^1)_{uv} x_u x_v^* (1 - \text{sgn}(|A_{uv} - A_{vu}|)) \\ &= \sum_{u,v=1}^n |(A_s^1)_{uv}| |x_u|^2 + \sum_{u,v=1}^n |(A_s^1)_{vu}| |x_v|^2 \\ &\quad - 2 \sum_{u,v=1}^n (A_s^1)_{uv} x_u x_v^* (1 - \text{sgn}(|A_{uv} - A_{vu}|)) \\ &= \sum_{u,v=1}^n |(A_s^1)_{uv}| |x_u|^2 + \sum_{u,v=1}^n |(A_s^1)_{uv}| |x_v|^2 \\ &\quad - 2 \sum_{u,v=1}^n (A_s^1)_{uv} x_u x_v^* (1 - \text{sgn}(|A_{uv} - A_{vu}|)) \\ &= \sum_{u,v=1}^n |(A_s^1)_{uv}| |x_u|^2 + \sum_{u,v=1}^n |(A_s^1)_{uv}| |x_v|^2 \\ &\quad - 2 \sum_{u,v=1}^n |(A_s^1)_{uv}| \text{sgn}((A_s^1)_{uv}) x_u x_v^* (1 - \text{sgn}(|A_{uv} - A_{vu}|)) \\ &= \sum_{u,v=1}^n |(A_s^1)_{uv}| (|x_u|^2 + |x_v|^2 - 2 \text{sgn}((A_s^1)_{uv}) x_u x_v^* (1 - \text{sgn}(|A_{uv} - A_{vu}|))) \\ &\geq \sum_{u,v=1}^n |(A_s^1)_{uv}| (|x_u| - \text{sgn}((A_s^1)_{uv}) |x_v|)^2 \geq 0. \end{aligned}$$

This shows, as desired, that  $L^\vartheta \succeq 0$ . Let us now consider the *normalized Quaternionic Laplacian*, which, according to Eq. (2), is defined as  $L_{\text{norm}}^\vartheta = \bar{D}_s^{-\frac{1}{2}} L^\vartheta \bar{D}_s^{-\frac{1}{2}}$ . We need to show that  $x^* L_{\text{norm}}^\vartheta x \geq 0$  for all  $x \in \mathbb{H}^n$ . Letting  $y = \bar{D}_s^{-\frac{1}{2}} x$ , we have  $x^* L_{\text{norm}}^\vartheta x = x^* \bar{D}_s^{-\frac{1}{2}} L^\vartheta \bar{D}_s^{-\frac{1}{2}} x = y^* L^\vartheta y$ . As the latter quantity was proven before to be nonnegative for all  $y \in \mathbb{H}^n$ ,  $L_{\text{norm}}^\vartheta \succeq 0$  follows.  $\square$

**Theorem 5.**  $\lambda_{\max}(L_{\text{norm}}^\vartheta) \leq 2$ .

*Proof.* As the Courant-Fischer theorem applied to  $L_{\text{norm}}^\vartheta$  implies:

$$\lambda_{\max} = \max_{x \neq 0} \frac{x^* L_{\text{norm}}^\vartheta x}{x^* x},$$

we need to show that the following holds:

$$\max_{x \neq 0} \frac{x^* L_{\text{norm}}^\vartheta x}{x^* x} \leq 2.$$

For the purpose, let  $B := \bar{D}_s + H^\vartheta$  and let  $B_{\text{norm}} := \bar{D}_s^{-\frac{1}{2}} B \bar{D}_s^{-\frac{1}{2}}$  be its normalized counterpart. Assuming  $B_{\text{norm}} \succeq 0$ , we would deduce the following for all  $x \in \mathbb{H}^n$ :

$$x^* B_{\text{norm}} x \geq 0 \Leftrightarrow x^* \left( I + D^{-\frac{1}{2}} H^\vartheta D^{-\frac{1}{2}} \right) x \geq 0 \Leftrightarrow$$

$$\begin{aligned}
& -x^* D^{-\frac{1}{2}} H^\vartheta D^{-\frac{1}{2}} x \leq x^* x \Leftrightarrow \\
& x^* I x - x^* D^{-\frac{1}{2}} H^\vartheta D^{-\frac{1}{2}} x \leq 2x^* x.
\end{aligned}$$

This would suffice to prove the claim as  $x^* I x - x^* D^{-\frac{1}{2}} H^\vartheta D^{-\frac{1}{2}} x \leq 2x^* x$  implies that  $\frac{x^* L_{\text{norm}}^\vartheta x}{x^* x} \leq 2$  holds for all  $x \in \mathbb{H}^n$ .

Letting  $y = \bar{D}_s^{-\frac{1}{2}} x$ , we observe that  $x^* B_{\text{norm}} x = x^* \bar{D}_s^{-\frac{1}{2}} B \bar{D}_s^{-\frac{1}{2}} x \geq 0$  holds for all  $x \in \mathbb{H}^n$  if and only if  $y^* B y \geq 0$  holds for all  $y \in \mathbb{H}^n$ . Therefore, it suffices to show that  $B \succeq 0$ .

As  $B$  is Hermitian by construction, we have  $x^* \Im_1(B)x = x^* \Im_2(B)x = x^* \Im_3(B)x = 0$  for all  $x \in \mathbb{H}^n$ . Thus, we only need to show that  $x^* \Re(B)x \geq 0$  holds for all  $x \in \mathbb{H}^n$ . This is done via the following derivation:

$2x^* \Re(B)x$

$$\begin{aligned}
& = 2 \sum_{u,v=1}^n (\bar{D}_s)_{uv} x_u x_v^* + 2 \sum_{u,v=1}^n (A_s^1)_{uv} x_u x_v^* (1 - H_{uv}^0) \\
& = 2 \sum_{u,v=1}^n (\bar{D}_s)_{uv} x_u x_v^* + 2 \sum_{u,v=1}^n (A_s^1)_{uv} x_u x_v^* (1 - \text{sgn}(|A_{uv} - A_{vu}|)) \\
& = 2 \sum_{i=1}^n (\bar{D}_s)_{ii} x_i x_i^* + 2 \sum_{u,v=1}^n (A_s^1)_{uv} x_u x_v^* (1 - \text{sgn}(|A_{uv} - A_{vu}|)) \\
& = 2 \sum_{u,v=1}^n |(A_s^1)_{uv}| |x_u|^2 + 2 \sum_{u,v=1}^n (A_s^1)_{uv} x_u x_v^* (1 - \text{sgn}(|A_{uv} - A_{vu}|)) \\
& = \sum_{u,v=1}^n |(A_s^1)_{uv}| |x_u|^2 + \sum_{u,v=1}^n |(A_s^1)_{vu}| |x_v|^2 \\
& \quad + 2 \sum_{u,v=1}^n (A_s^1)_{uv} x_u x_v^* (1 - \text{sgn}(|A_{uv} - A_{vu}|)) \\
& = \sum_{u,v=1}^n |(A_s^1)_{uv}| |x_u|^2 + \sum_{u,v=1}^n |(A_s^1)_{uv}| |x_v|^2 \\
& \quad + 2 \sum_{u,v=1}^n (A_s^1)_{uv} x_u x_v^* (1 - \text{sgn}(|A_{uv} - A_{vu}|)) \\
& = \sum_{u,v=1}^n |(A_s^1)_{uv}| |x_u|^2 + \sum_{u,v=1}^n |(A_s^1)_{uv}| |x_v|^2 \\
& \quad + 2 \sum_{u,v=1}^n |(A_s^1)_{uv}| \text{sgn}((A_s^1)_{uv}) x_u x_v^* (1 - \text{sgn}(|A_{uv} - A_{vu}|)) \\
& = \sum_{u,v=1}^n |(A_s^1)_{uv}| (|x_u|^2 + |x_v|^2 + 2 \text{sgn}(A_{uv}) x_u x_v^* (1 - \text{sgn}(|A_{uv} - A_{vu}|))) \\
& \geq \sum_{u,v=1}^n |(A_s^1)_{uv}| (|x_u|^2 + |x_v|^2) \geq 0.
\end{aligned}$$

This concludes the proof.  $\square$

## C QuaterGCN's architecture

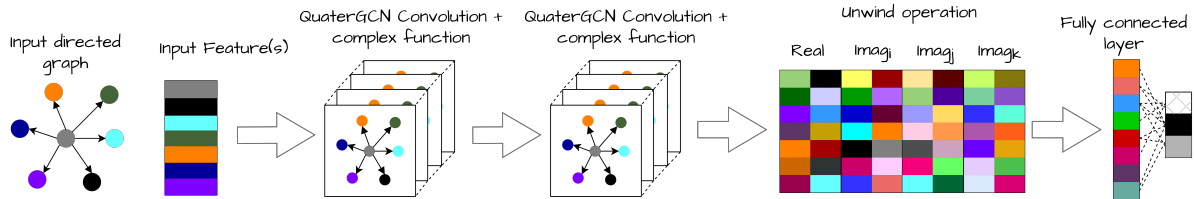


Figure 2: Overview of QuaterGCN

Based on the task to be solved, QuaterGCN features one or more convolution layers followed by either a linear layer with weights  $W$  or a 1D convolution. Considering, for example, a node-classification task of predicting which of a set of unknown classes a graph vertex belongs to, QuaterGCN implements the function

$$\text{unwind} \left( Z^{\vartheta(2)} \left( Z^{\vartheta(1)} \left( X^{(0)} \right) \right) \right) W,$$



where  $X^{(0)} \in \mathbb{H}^{n \times c}$  is the input feature matrix,  $Z^{\mathfrak{q}(1)} \in \mathbb{H}^{n \times f_1}$  and  $Z^{\mathfrak{q}(2)} \in \mathbb{H}^{n \times f_2}$  are two convolutional layers, and  $W \in \mathbb{H}^{4f_2 \times d}$  are the weights of the linear layer (with  $d$  being the number of classes).

Fig. 2 illustrates the structure of the proposed QuaterGCN network for the node-classification task.

## D Further Details on the Datasets

**Real-World Datasets.** We tested QuaterGCN on six real-world datasets: Bitcoin-OTC and Bitcoin Alpha [Kumar et al., 2016]; Slashdot and Epinions Leskovec et al. [2010]; WikiRfa [West et al., 2014]; and Telegram [Bovet and Grindrod, 2020].

Bitcoin-OTC and Bitcoin Alpha are built from exchange operations executed within the Bitcoin-OTC and Bitcoin Alpha platforms, which were rated by the users with values between  $-10$  to  $+10$  ( $0$  is not allowed). Scammers are given a score of  $-10$ . A score of  $+10$  indicates full trust. Values in between indicate intermediate evaluations.

The other two datasets are Slashdot and Epinions. The first comes from a tech news website with a community of users. The website introduced Slashdot Zoo features that allow users to tag each other as friend or foe. The dataset represents a signed social network with friend ( $+1$ ) and enemy ( $-1$ ) labels. Epinions is an online who-trust-who social network of a consumer review site (*Epinions.com*). Site members can indicate their trust or distrust of other people’s reviews. The network reflects people’s views on others.

WikiRfa is a collection of votes given by Wikipedia members gathered from 2003 to 2013. Indeed, any Wikipedia member can vote for support, neutrality, or opposition to a Wikipedia editor’s nomination for administrator. This leads to a directed, multigraph (unrestricted in sign) in which nodes represent Wikipedia members and edges represent votes, which is then transformed into a simple graph by condensing any parallel edges into a single edge of weight equal to the sum of the weights of the original edges. The graph features a higher number of nodes and edges than the one proposed in Huang et al. [2021]. In these five datasets, the classes of positive and negative edges are imbalanced (see Table 7).

Telegram models an influence network built on top of interactions among distinct users who propagate ideologies of a political nature. The graph encompasses 245 Telegram channels with 8912 links, with labels of four classes generated as explained in Bovet and Grindrod [2020].

Table 7: Statistics of the six datasets

Data set	$n$	$ \varepsilon^+ $	$ \varepsilon^- $	% pos	Directed	Weighted	Density	Undirected Edges	Antiparallel Edges with different/opposite weight
Telegram	245	8,912	0	100.00	✓	✓	14.91%	2.22%	15.42%
Bitcoin-Alpha	3,783	22,650	1,536	93.65	✓	✓	0.17%	59.57%	23.63%
Bitcoin-OTC	5,881	32,029	3,563	89.99	✓	✓	0.10%	56.89%	22.34%
WikiRfa	11,381	138,143	39,038	77.97	✓	✓	0.14%	5.27%	2.14%
Slashdot	82,140	425,072	124,130	77.70	✓	✗	0.01%	17.03%	0.71%
Epinion	131,828	717,667	123,705	85.30	✓	✗	0.01%	30.16%	0.64%

**Synthetic Datasets.** The synthetic graphs we adopted belong to two classes:

1. DBSM: graphs obtained via a direct stochastic block model (DSBM) following Fiorini et al. [2022], with edge weights taking integer values in  $\{2, 1000\}$ .
2. Di150 and Di500: since the DBSM graphs do not contain any digons, we introduce a second class of synthetic graphs with a variable percentage of digons  $\delta \in (0, 1)$  with edge weights taking integer values in  $\{2, 4\}$ . Di150 contains graphs with 150 nodes per cluster, whereas Di500 contains graphs with 500 nodes per cluster.

For the DBSM graphs, we select a number of nodes in each cluster  $N$  and a number of clusters  $C$  by which the vertices are partitioned into groups of equal size. We introduce a set of probabilities  $\{\alpha_{uv}\}_{1 \leq u, v \leq C}$ , where  $0 \leq \alpha_{uv} \leq 1$  with  $\alpha_{uv} = \alpha_{vu}$ . Such values coincide with the probability of generating an undirected edge between nodes  $u$  and  $v$  taken from different clusters.  $\alpha_{uu}$  is the probability of generating an undirected edge between nodes in the same cluster. As these graphs are undirected, we follow Fiorini et al. [2022] and introduce a rule to transform the graph from undirected to directed: we define a collection of probabilities  $\{\beta_{uv}\}_{1 \leq u, v \leq C}$  with  $0 \leq \beta_{uv} \leq 1$  such that  $\beta_{uv} + \beta_{vu} = 1$ . Each edge  $\{u, v\}$  is assigned a direction using the rule that the edge goes from  $u$  to  $v$  with probability  $\beta_{uv}$  and from  $v$  to  $u$  with probability  $\beta_{vu}$ .

For the creation of the Di150 and Di500 graphs, we introduce an additional set of probabilities  $\delta$  with  $0 < \delta < 1$  that specify what percentage of edges from those generated by the aforementioned procedure should be preserved as undirected; all the other edges are transformed into a digon.

## E Experiment Details

**Hardware.** The experiments were conducted on 3 different machines: the first features 1 NVIDIA Tesla T4 GPU, 380 GB RAM, and Intel(R) Xeon(R) Gold 6238R CPU @ 2.20GHz CPU; the second features 1 NVIDIA RTX 3090 GPU, 64 GB RAM, and 12th Gen Intel(R) Core(TM) i9-12900KF CPU @ 3.20GHz CPU; the third features 1 NVIDIA Ampere A100, 384 GB RAM, and 2x Intel(R) Xeon(R) Silver 4210 CPU @ 2.20GHz Sky Lake CPU.

**Model Settings.** We train every learning model considered in this paper for up to 3000 epochs with early stopping whenever the validation error does not decrease after 500 epochs for node classification and three-class edge prediction tasks. For the four-class edge prediction task and the five-class edge prediction task, we set the number of epochs to 300 for Bitcoin\_Alpha, Bitcoin\_OTC and WikiRfa, while 500 epochs for Slashdot and Epinions. Following Fiorini et al. [2022], we add a single dropout layer with a probability of 0.5 before the last layer. We set the parameter  $K$  adopted in ChebNet, MagNet, SigMaNet, QGNN, and QuaterGCN to 1. We adopt a learning rate of  $10^{-3}$  for the node classification task and the three-class edge prediction task, whereas for the other two tasks (4/5CEP), we use a learning rate of  $10^{-2}$ . We employ the optimization algorithm ADAM with weight decays equal to  $5 \cdot 10^{-4}$  (in order to avoid overfitting). For SGCN, SNEA, SiGAT, and SDGNN, we use the same setting proposed in He et al. [2022b].

A hyperparameter optimization procedure is adopted to identify the best set of parameters for each model. In particular, we tune the number of filters by selecting it in  $\{16, 32, 64\}$  for the graph convolutional layers of all models except for DGCN.

Some further hyperparameter values are:

- MagNet’s coefficient  $q$  is chosen in  $\{0.01, 0.05, 0.1, 0.15, 0.2, 0.25\}$ .
- The coefficient  $\alpha$  used in the PageRank-based models APPNP and DiGraph takes values in  $\{0.05, 0.1, 0.15, 0.2\}$ .
- For APPNP, we set  $K = 10$  for the node-classification task (following Klicpera et al. [2019]) and take  $K$  in  $\{1, 5, 10\}$  for the three-class edge prediction task.
- For GAT, we select the number of heads in  $\{2, 4, 8\}$ .
- For DGCN, the number of filters per channel takes values in  $\{5, 15, 30\}$ .
- In GIN, the parameter  $\epsilon$  is set to 0.
- In SSSNET, the parameters  $\gamma_s$  and  $\gamma_t$  are set to 50 and 0.1, respectively. 10% of the nodes per class are taken as seed nodes.
- In ChebNet, GCN, and QGNN, we employ the symmetrized adjacency matrix defined as  $A_s = \frac{A+A^\top}{2}$ .
- For DiGCL, we select *Pacing function* in  $[linear, exponential, logarithmic, fixed]$  using two settings: i)  $\tau = 0.4$ , *drop feature rate 1* = 0.3 and *drop feature rate 2* = 0.4, and ii)  $\tau = 0.9$ , *drop feature rate 1* = 0.2 and *drop feature rate 2* = 0.1.
- MSGNN’s coefficient  $q$  is chosen in  $\{0.2q_0, 0.4q_0, 0.6q_0, 0.8q_0, q_0\}$ , where  $q_0 := 1/[2 \max_{u,v}(A_{uv} - A_{vu})]$ .

**Node Classification Task.** For the Telegram dataset, we retain the dataset’s original features. When experimenting with the synthetic datasets, the feature vectors are generated using the in-degree and out-degree procedure described before.

**Three-Class Edge Prediction Task.** The feature matrix  $X \in \mathbb{R}^{n \times 2}$  is defined in such a way that  $X_{u1}$  corresponds to the in-degree of node  $u$  and  $X_{u2}$  to node  $u$ ’s out-degree, for all  $u \in N$ . This allows the models to learn structural information directly from the adjacency matrices.

**Four/Five-Class Edge Prediction Task.** The feature matrix  $X \in \mathbb{R}^{n \times 2}$  is defined as in three class edge prediction task. However, for these tasks, the in-degree and out-degree are computed using the absolute values of their corresponding edge weights.

## F More Experiments

For completeness, we report the results obtained for the three-class edge prediction task on the Di500 graphs in Table 8. We omitted these results from Subsection *Three-Class Edge Prediction Task (3CEP)* since, as the table shows, on such graphs all the methods achieve a performance close to 33% (i.e., close to what a purely random model would achieve)—in essence, the methods’ predictive capabilities do not deviate significantly from what one would anticipate via a completely random prediction and, as such, these results are not particularly interesting.

Table 8: Accuracy (%) on datasets of the three class edge prediction task

	Three Class Edge prediction		
	Di500		
	$\delta = 0.2$	$\delta = 0.5$	$\delta = 0.7$
ChebNet	34.21 $\pm$ 0.01	35.14 $\pm$ 0.01	35.48 $\pm$ 0.03
GCN	34.22 $\pm$ 0.01	35.15 $\pm$ 0.01	35.49 $\pm$ 0.02
QGNN	34.22 $\pm$ 0.01	35.15 $\pm$ 0.01	35.49 $\pm$ 0.02
APNP	34.21 $\pm$ 0.01	35.13 $\pm$ 0.01	35.48 $\pm$ 0.02
SAGE	34.18 $\pm$ 0.02	35.12 $\pm$ 0.01	35.46 $\pm$ 0.02
GIN	34.08 $\pm$ 0.02	35.13 $\pm$ 0.01	35.48 $\pm$ 0.01
GAT	34.21 $\pm$ 0.02	35.14 $\pm$ 0.01	35.48 $\pm$ 0.02
DGCN	34.21 $\pm$ 0.02	35.14 $\pm$ 0.02	35.48 $\pm$ 0.02
DiGraph	34.62 $\pm$ 0.16	34.76 $\pm$ 0.19	35.16 $\pm$ 0.15
DiGCL	32.89 $\pm$ 0.01	32.43 $\pm$ 0.01	32.25 $\pm$ 0.01
MagNet	35.06 $\pm$ 0.14	35.02 $\pm$ 0.08	35.44 $\pm$ 0.03
SigMaNet	34.93 $\pm$ 0.14	34.78 $\pm$ 0.01	35.16 $\pm$ 0.12
QuaterGCN	35.07 $\pm$ 0.19	34.74 $\pm$ 0.06	35.25 $\pm$ 0.09